Biomaterials Advances 159 (2024) 213801

Contents lists available at ScienceDirect

Biomaterials Advances

journal homepage: www.journals.elsevier.com/materials-science-and-engineering-c

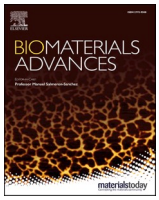

Towards bone regeneration: Understanding the nucleating ability of proline-rich peptides in biomineralisation

Øystein Øvrebø [a,b,c], Angela De Lauretis [a,b], Qianli Ma [a], Ståle Petter Lyngstadaas [a], Giuseppe Perale [d,e,f], Ola Nilsen [g], Filippo Rossi [b], Håvard J. Haugen [a,*]

[a] Department of Biomaterials, Institute of Clinical Dentistry, University of Oslo, 0318 Oslo, Norway
[b] Department of Chemistry, Materials and Chemical Engineering "Giulio Natta", Politecnico di Milano, 20133 Milano, Italy
[c] Material Biomimetic AS, Oslo Science Park, 0349 Oslo, Norway
[d] Industrie Biomediche Insubri SA, Mezzovico-Vira 6805, Switzerland
[e] Faculty of Biomedical Sciences, University of Southern Switzerland, Lugano 6900, Switzerland
[f] Ludwig Boltzmann Institute for Experimental and Clinical Traumatology, Donaueschingenstrasse 13, 1200 Vienna, Austria
[g] Centre for Materials Science and Nanotechnology, Department of Chemistry, University of Oslo, Gaustadalléen 21, NO-0349 Oslo, Norway

ARTICLE INFO

Keywords:
Biomineralisation
Disordered peptides
Bone regeneration
Molecular dynamics
Regenerative medicine

ABSTRACT

Obtaining rapid mineralisation is a challenge in current bone graft materials, which has been attributed to the difficulty of guiding the biological processes towards osteogenesis. Amelogenin, a key protein in enamel formation, inspired the design of two intrinsically disordered peptides (P2 and P6) that enhance in vivo bone formation, but the process is not fully understood. In this study, we have elucidated the mechanism by which these peptides induce improved mineralisation. Our molecular dynamics analysis demonstrated that in an aqueous environment, P2 and P6 fold to interact with the surrounding Ca^{2+}, PO_4^{3-} and OH^- ions, which can lead to apatite nucleation. Although P2 has a less stable backbone, it folds to a stable structure that allows for the nucleation of larger calcium phosphate aggregates than P6. These results were validated experimentally in a concentrated simulated body fluid solution, where the peptide solutions accelerated the mineralisation process compared to the control and yielded mineral structures mimicking the amorphous calcium phosphate crystals that can be found in lamella bone. A pH drop for the peptide groups suggests depletion of calcium and phosphate, a prerequisite for intrinsic osteoinduction, while S/TEM and SEM suggested that the peptide regulated the mineral nucleation into lamella flakes. Evidently, the peptides accelerate and guide mineral formation, elucidating the mechanism for how these peptides can improve the efficacy of P2 or P6 containing devices for bone regeneration. The work also demonstrates how experimental mineralisation study coupled with molecular dynamics is a valid method for understanding and predicting in vivo performance prior to animal trials.

1. Introduction

Bone graft material should exhibit osteoinductive properties for successful bone regeneration in large skeletal defects or procedures like spinal fusion [1,2]. Osteoinductive properties are traditionally described by a material's ability to recruit preosteoblast cells and stimulate them towards differentiation, thereby increasing the rate of bone formation [3,4]. Lately, it has been established that a material can claim intrinsic osteoinductive properties if it can create a local depletion of calcium and/or phosphate through binding to the ions [5]. This indicates that osteoinduction is not only a biologically driven phenomenon but is also affected by physical, spatial and chemical factors.

Part of the osteoinduction process is biomineralisation, i.e., hard tissue formation. Even if a material is osteoinductive, the deposited mineralisation must be organised to replicate native bone. This is challenging as bone is a composite of minerals and collagen hierarchically structured down to the nanoscale [6]. The hierarchical organisation of the composite structure has been recognised to give bone its unique properties of combined high compressive strength and fracture toughness [7–9]. Hence, a suitable bone graft material must guide the mineralisation structure and induce mineral precipitation. Recently, Pang et al. [10] studied the bone structure on a nanoscale and determined that the bone consists of stacks of mineral lamellar that are "glued" together by non-collagenous proteins, which they believe

* Corresponding author at: Department of Biomaterials, Institute of Clinical Dentistry, University of Oslo, 0318 Oslo, Norway.
E-mail address: h.j.haugen@odont.uio.no (H.J. Haugen).

https://doi.org/10.1016/j.bioadv.2024.213801
Received 8 December 2023; Received in revised form 26 January 2024; Accepted 18 February 2024
Available online 21 February 2024

contributes to the bone stiffness, strength and ability to absorb energy.

The biomineralisation process is governed by hormones, enzymes, and regulatory proteins [11,12]. To understand this mechanism, Kalmar and colleagues extensively analysed the SwissProt protein database proteins responsible for biomineralisation in vertebrates [11]. They observed that these proteins had an extremely high level of predictable disorder compared to other protein groups and a high frequency and repetition of the amino acids serine, arginine, and proline. Their results suggest that these proteins' ordered-disordered nature is essential in mineralisation. Proteins with such properties are called intrinsically disordered proteins (IDPs). One such IDP is amelogenin, which is associated with the formation of enamel in vertebrates [13–15], where it is believed that the proline-richness (approx. 30 %) prevents the formation of secondary structures and provides the IDP characteristics [16]. Inspired by amelogenin's role in regulating biomineralisation and composition of proline-enriched regions, a set of artificial peptide sequences was designed [17]. These peptides were investigated in a set of in vitro comparative studies to the animal-derived enamel matrix derivative (EMD) [17–20]. EMD is a protein-cocktail (90 % amelogenin) commercially used for periodontal regeneration in Emdogain®, a product by Institute Straumann AG [21]. In their initial study, Rubert and colleagues observed that the P2 peptide (see Table 1 [22]) gave higher expression for all osteoblast gene markers except for collagen type 1 when tested on human umbilical cord mesenchymal stem cells [17]. Further, P2 also increased the calcium deposition rate compared to EMD. In a later study, another sequence, P6 (see Table 1), showed an ability similar to the P2 peptide and EMD to induce osteoblastic differentiation [19]. Since the in vitro results for bone formation were particularly promising for two of the peptides, P2 and P6, they were investigated as enhancing bone formatting peptides by being integrated into the coating of the new bone xenohybrid graft SmartBonePep® [23].

Both on osteoblasts [24] and human mesenchymal stem cells [25], the SmartBonePep® graft exhibit improved cell proliferation and promotes osteogenic-related gene expression. Continuing on this work, Rahmati and colleagues recently tested the SmartBonePep® graft in vivo in a critical-sized bone defect model in young pig skulls [26]. Their results suggest that P2 stimulates significantly greater biomineralisation than P6 and the bone graft without peptide, as confirmed by histology, immunohistochemistry and micro-Computed Tomography (μCT). Interestingly, Synchrotron WAXS/SAXS results indicate that the P2 group had an apparent ability to remodel itself into native-like bone compared to the other groups. Their optical photothermal IR microscopy results suggest that the peptides are present in the highly mineralised regions of the treated defect. Therefore, it can be hypothesised that the peptides help nucleate the mineral structures.

A remaining question is whether the peptides obtain their effect through the stimulation of cells or by physical, spatial, or chemical means. Consequently, in this paper, we aim to investigate the ability of two proline-rich peptides (P2 and P6) to regulate biomineralisation. This was done using molecular dynamics simulation to understand the peptides' ability to bind to calcium, phosphate, and hydroxide ions, thereby nucleating mineral crystals. To validate the molecular dynamics simulation, the peptides were introduced to a concentrated simulated body fluid solution that was developed by researchers at the RMS Foundation to favour mineralisation [27]. Calcium and phosphate concentrations were measured at different time points, and the precipitated mineralisation was characterised using TEM, XRD, S/TEM with EDS and SEM.

Table 1
Peptide sequences of the two peptide variants; P = Proline, L = Leucine, V = Valine, S = Serine, Q = Glutamine, M = Methionine, H = Histidine – Covered by the patent: [22].

Peptide	Peptide sequences
P2	PLV PSQ PLV PSQ PLV PSQ PQ PPLPP
P6	PHQ PMQ PQP PVH PMQ PLP PQ PPLPP

2. Materials and methods

2.1. Materials

The proline-rich IDPs, P2 and P6 (sequences in Table 1 [22]), were supplied by Pepmic Co., Ltd., Jiangsu, China. All other chemicals were acquired from VWR, Oslo, Norway.

2.2. Molecular dynamics simulation

An atomistic model of the P2 and P6 peptides immersed in an aqueous hydroxyapatite-ion (Ca^{2+}, PO_4^{3-}, OH^-) solution was developed in Biovia Discovery Studio v17.2.0 using a "OPLS 2005" all-atom force field. Initially, one of the peptides is in its extended orientation surrounded by randomly placed clusters of hydroxyapatite-ions, with the water (TIP3P model) molecules at 10 Ångström (Å). The distinctive 7.7 pH environment was created by altering the protonation state of titration sites. The pK_a values for each peptide protonation site were predicted using the 'Prepare protein wizard' and Simulation setup modules of Schrödinger's Desmond. These peptide models were then simulated to obtain the equilibrated configuration for the peptides in an aqueous solution. After preliminary minimisation, the model systems were heated for 100 ps in an orthorhombic ensemble molecular dynamic (MD) simulation run to reach the experimental temperature of 27 °C (300 K). During this step, the water molecules were kept fixed. All restraints were removed, and the peptides were simulated by running 100 ns of an isothermal–isobaric MD simulation at 300 K of temperature and 1 atm of pressure under periodic boundary conditions. A RESPA integrator was used with a time step of 2 fs, and long-range electrostatics were computed every 6 fs. One system for each of the two simulations containing approximately 18,050 and 17,658 atoms for P2 & P6 peptides was equilibrated using Desmond in the NPT ensemble. The final simulation system consisted of P2/P6 peptide, 65 Ca^{2+} ions, 39 PO_4^{3-} ions, 13 OH^- ions, and 5794 and 5660 water molecules, respectively, for P2 & P6 peptides. These MD runs used a time step of 2 femtoseconds, the Langevin thermostat, and a 9 Å cutoff. The particle mesh Ewald5 (PME) approach was used to treat the long-range electrostatic effects, and the SHAKE algorithm was used to treat the bonds involving hydrogen atoms. Simulation Quality analysis (SQA), Simulation event analysis (SEA) and Simulation interaction diagram modules of Schrödinger's Desmond package were employed to analyse the simulation and to generate the graphs.

2.3. Mineralisation assay

The mineralisation study used the concentrated simulated body fluid developed by Maazouz and colleagues [27], which we coined RMS-SBF. Two stock solutions were prepared using sodium chloride, calcium chloride, disodium phosphate and Milli-Q water: one calcium-rich (SBF-A) and one phosphate-rich (SBF-B) after the ion concentration described in Table 2. The simulated body fluid used for the mineralisation study (RMS-SBF) was prepared by mixing SBF-A and SBF-B in equal volumes just prior to the test. For the experiment, the RMS-SBF solution with peptides and control without peptides was put in vials (3 ml) and filled completely to exclude CO_2. The peptides were, prior to addition, dissolved in 1 % acetic acid at a concentration of 10 mg/ml and were added to the RMS-SBF for a final concentration of 10 μg/ml. The peptide stock solution was stored in the fridge (4 °C) and used within 7 days of

Table 2
Ion solution in the different SBF solutions – all in mM.

	Na^+	Ca^{2+}	Cl^-	HPO_4^{2-}
SBF-A	161.2	7.4	176.0	
SBF-B	161.2		152.8	4.2
RMS-SBF	161.2	3.7	164.4	2.1

preparation.

Before starting the experiment, the pH of RMS-SBF was measured with a PHM210 Standard pH meter (MeterLab®, Radiometer Analytical SAS, France) equipped with a pH sensor from VWR Chemicals, US.

The vials were left on a shaking plate at 50 rpm for 3 h, 6 h, 12 h, 24 h, and 48 h. After that, the samples were filtered under vacuum through a 0.22 μm mixed cellulose esters membrane filter paper (Merck Millipore Ltd., Ireland) to separate the precipitate. The pH of the filtrate was measured before the remaining calcium and phosphorous concentration was measured using Inductively Coupled Plasma Mass Spectroscopy (ICP-MS). The filter paper was air-dried, before the precipitate was investigated using Scanning Electron Microscopy (SEM), X-ray Diffraction Spectroscopy (XRD), Transmission Electron Microscopy (TEM), and S/TEM coupled with Energy Dispersive X-ray Spectroscopy (EDS). The precipitation was dispersed in ethanol to prepare the samples for this analysis and transferred to a copper grid (300 μm mesh with 25 μm grid and carbon film – Agar Scientific).

2.4. TEM & S/TEM

The precipitate was dispersed in ethanol and then put on a TEM grid to perform the analysis. Transmission electron microscopy was performed at 200 kV and 134 μA (dark current: 95 μA) with a JEM-2100F machine (JEOL Ltd., Japan). Scanning transmission electron microscopy analysis was performed at 300 kV with a Titan G2 60–300 machine (FEI Company, US). Two types of detectors were used to collect the images: HAADF (high-angle annular dark-field) and BF (bright-field). The S/TEM was also combined with EDS to identify material composition.

2.5. SEM

For Scanning Electron Microscopy, a SU8230 (Hitachi, Japan) was used at 1 kV, 10 μA, and a working distance of 4.6 mm. The images were acquired using a combination of secondary and back-scattering electrons, and with a deceleration of the electrons. The TEM grids were put on the carbon tape on top of a SEM aluminium stub to carry out the analyses.

2.6. ICP-MS

An Agilent 7700 ICPMS/MS (Agilent Technologies, Santa Barbara, California, USA) was used to analyse Ca and P concentrations. The ICPMS/MS was run in He and H_2 gas collision mode and no gas mode for analyses. All reported concentrations have been normalised to sample mass. The samples were analysed with 1/10 dilution with HNO_3 as conservation fluid. Analyses were performed with two different parameters. No gas mode ICPMS/MS analysis was performed with the following parameters: RF Power: 1550 W, RF Matching 1.80 Hz, No Gas Mode, Peristaltic Pump: 0.1 rps, Makeup Gas: 0.12 ml/min, and Carrier Gas: 1.10 l/min. Helium gas collision mode ICPMS/MS analysis was performed with the following parameters: RF Power: 1550 W, RF Matching 1.80 Hz, Peristaltic Pump: 0.1 rps, Makeup Gas: 0.12 ml/min, H2 Gas: 6.00 l/min, and He Collision Gas: 5.0 ml/min. The method used has been based on EN ISO17294-1:2007 and EN-ISO17294-2:2016.

2.7. XRD

X-ray diffraction for structural analysis was carried out on an AXS D8 Discover (Bruker) diffractometer, equipped with a LynxEye strip detector and a Ge (111) focusing monochromator, providing CuKα1 ($\lambda = 1.5406$ Å) radiation.

2.8. Statistical analysis

For the pH and ICP-MS data, statistical analysis between the groups was conducted with a one-tailed Welch's *t*-test. It was assumed normality and alpha was set as 0.05.

3. Results

In this study, molecular dynamics and an experimental mineralisation study have been implemented to elucidate the mechanism for which two proline-rich, intrinsically disordered peptides, P2 and P6, favour mineralisation (Fig. 1).

3.1. Molecular simulation of peptides

The P2 and P6 peptides have polar and hydrophobic amino acids but consist of a series of polar and hydrophobic amino acids (whole sequences in Table 1). However, some key differences are that P2 consists of serine (polar) amino acids. Meanwhile, P6 is composed of histidine (polar) and methionine (hydrophobic) amino acids. The model consisted of an aqueous environment with calcium phosphate ions (Fig. 1). The analysis revealed that both P2 & P6 peptides molecular dynamic systems were observed to maintain the 300 K temperature; approx. 0 atm pressure and overall simulation box volume as 180,000 & 175,000 Å cubes with 18,050 and 17,658 total number of atoms including 5794 and 5660 water molecules, respectively (Fig. S1). The simulation was done over a 100 ns timespan. Considering the first and last frame, the P2 peptide was more stretched than the P6. Meanwhile, visual inspection of the last frame reveals that the P6 peptide is folding itself spontaneously faster than the P2 peptide via forming strong interactions with Ca^{2+}, PO_4^{3-} and OH^- ions (Fig. 1A). It can be observed that the P2 folds to form intramolecular bonds in a stable structure.

These observations are supported by the fact that P2 forms a higher number of intramolecular hydrogen bonds than P6, while P6 forms a higher number of intermolecular hydrogen bonds (Fig. 2A & B). In general, more intramolecular hydrogen bonds increase the structure stability, limiting the ability to interact with other micro or macromolecules. Thus, the P6 peptide has more flexibility and open residues to interact with other micro or macromolecules. If we evaluate the energy levels (Fig. 2C), we can observe that P6 had a mean energy level of -2540 ± 59 KCal/Mol and P2 of -1196 ± 82 KCal/Mol, where a lower energy level favours thermodynamic, structural stability and chemical process. We can further see that both peptides have a decrease in the radius of gyration (RoG - Fig. 2D), which indicates that they fold. This folding is particularly evident for P2, which has an apparent fall from 16 to 18 Å down to approx. 10 Å, it is then stable there for around 20 ns before it starts increasing and fluctuating after 40 ns. Concurrently, there is a jump in inter and intra-interaction for P2 (Figs. 2A & B, 3E). P6 has a steadier change in RoG, and there are no sudden upticks in interactions. If we consider the Root-Mean-Square Deviation (RMSD) of the peptide backbone (Fig. 2E), it can be observed that, initially, the RMSD value for both peptides quickly increases, suggesting much movement in the start-up to 30 ns. Between 30 and 40 ns, P2 has two prominent fluctuation peaks reaching values up to 17.9 Å before stabilising. In comparison, P6 reaches a maximum RMSD of 12.9 Å, which is less than 75 % of the maximum RMSD observed for P2. Ultimately, P2 stabilises at a higher RMSD value P6 (mean of 15.7 Å versus 11.8 Å, respectively, between 40 and 100 ns). When evaluating the RMS Fluctuation (RMSF Fig. 2F), peaks around the C- and N-terminus for both peptides can be observed. For P2, there is also a clear peak around residue 11 (Serine). After the folding, residues 10–13 form a new far end on the P2 peptide, which can explain the fluctuation. The same is the case for P6, where the residues 12–14 are at the far end of the fold and exhibit the fluctuation peak.

When evaluating the visual images from the simulation, it can be observed that through the glutamine (20th amino acid in sequence), the P2 peptide seems to nucleate a larger cluster of calcium phosphate ions. Although the P6 peptide appears to interact with more ions, it does not seem to nucleate large clusters like P2 did. We used Schrödinger's

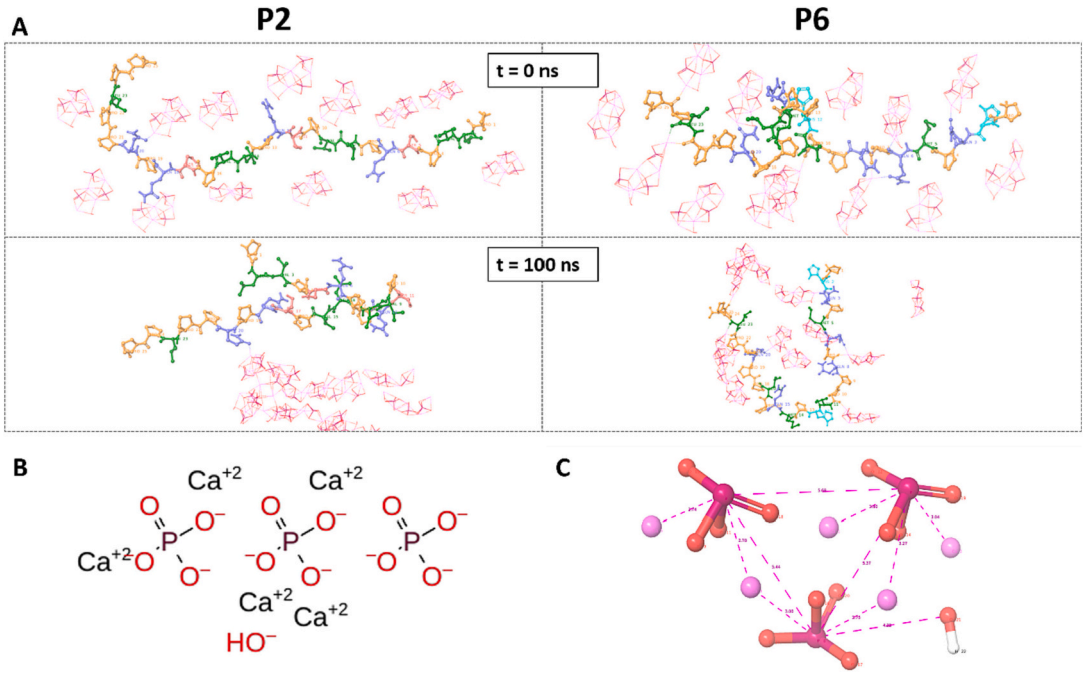

Fig. 1. Molecular dynamics model used for analysing the interaction between the peptides P2 and P6, and an aqueous environment enriched with Ca^{2+}, PO_4^{3-}, and OH^- ions. A Still frame image of the model at the start and end of the simulation (100 ns). The red clusters are the hydroxyapatite-related ions. B illustrates the 2D schematic representation of the ions' arrangement, and C illustrates these clusters as an energy-minimised 3D ball & stick representation of the arrangement of the ions with distance calculated in angstrom units.

Desmond software to investigate the interactions between the peptides and the Ca^{2+}, PO_4^{3-} and OH^- ions in detail. The analysis determined that 22 of the residues of P2 and 19 of the P6 residues were involved in peptide-ligand interactions (Fig. 3A & B). For P2, this involved 7 hydrogen bonds, 2 hydrophobic interactions, 18 water-bridging interactions and 1 ionic interaction, and for P6, this involved 5 hydrogen bonds, 2 hydrophobic interactions, 19 water-bridging interactions and two ionic bonds.

The lower panel of Fig. 3C & D interaction fraction is displayed for the residues. The interaction fracture measures the fraction of the simulation time the specific interaction is maintained. So, when one residue has multiple interactions of the same or different peptide-ligand interaction, the total interaction fraction could add up to more than 100 %. This is the case for the Gln_8-residue of the P6 peptide, where there are multiple water-bridges in addition to hydrogen bonds. For P2, primarily Pro_1 and Gln_20 residues have a fraction above 40 %. Furthermore, it is the Gln_20 residue that seems to nucleate the calcium phosphate cluster observed in Fig. 1A. Interestingly, most of the interaction for the Gln_20 residue appears to be water bridges and a minority of hydrogen bonds.

If we evaluate the number of contacts per residue over time, we can observe that P6 has a higher number of total connections than P2 over the investigated timespan, and the contacts are more stable (Fig. 3E & F). This agrees with the observed trends of energy, which suggest that P6 favours chemical interactions due to a more thermodynamically stable backbone.

3.2. Mineralisation study

The molecular dynamics were validated using a concentrated simulated body fluid solution coined RMS-SBF, where solutions with 10 μg/ml peptide were monitored for up to 48 h and controlled against the RMS-SBF without the peptides. The solution was measured for pH change and calcium and phosphate depletion before the mineralisation was characterised on a morphological and chemical level.

Although there was a pH drop for all groups, the pH drops at 3 h, 6 h, and 12 h for the P6 were significantly greater than for the control group (Fig. 4B). P6 also had a significantly greater pH drop than P2 at the 3 h time point. It has been previously established that a pH drop can be used as a proxy to measure mineralisation [28]. ICP-MS confirms that there is a depletion of calcium and phosphorous for all groups (Fig. 4). After 24 h, there can no longer be observed differences between the groups, and after 48 h, the control and P2 have a significantly lower pH than the P6 group.

SEM revealed precipitation in all groups but demonstrated differences in morphology between the groups (Fig. 5). The control group's mineralisation consisted of short crystallites with a seemingly large cross-section. Meanwhile, the peptide groups seem to form aggregated flake-like mineralisation, with significantly greater length than the crystallites of the control group. These flakes had the ability to stack on top of each other, similarly to lamella bone, which was particularly evident for P2. P2 had shorter crystallite flakes than P6, which could have made the stacking easier, allowing more compact mineralisation. We also noticed that P2 had more individual flakes. Meanwhile, P6 predominantly had aggregated flakes. Similar flakes were not observed for the control (Figs. 5A and S2).

We further investigated the samples in TEM and took the diffraction patterns to understand the crystallinity of the mineralisation. Meanwhile, the control group had shorter mineralisation crystals, the peptides, particularly P2, yielded longer crystals (Fig. 6A). However, all the diffraction patterns display clear concentric rings with similar diffraction intensity profiles, suggesting that all groups yield polycrystalline mineralisation. In Fig. 6B, we have plotted the rotational average diffraction pattern, allowing us to identify the material as apatite-based by comparing it to the x-ray pattern expected for a hexagonal calcium hydroxyapatite ($Ca_5[PO_4]_3[OH]$). There was no difference observed in the pattern, only in intensity. We also conducted an XRD analysis of the mineralisation on the filter paper. Since the cellulose filter paper gave a reflection, the signals had to be subtracted. We could still observe clear peaks around 31.8° and 45.5°, which are associated with the 211 and 203 hkl indices (Fig. 6C), which can also be observed in calcium hydroxyapatite reference material [29]. There was no clear difference

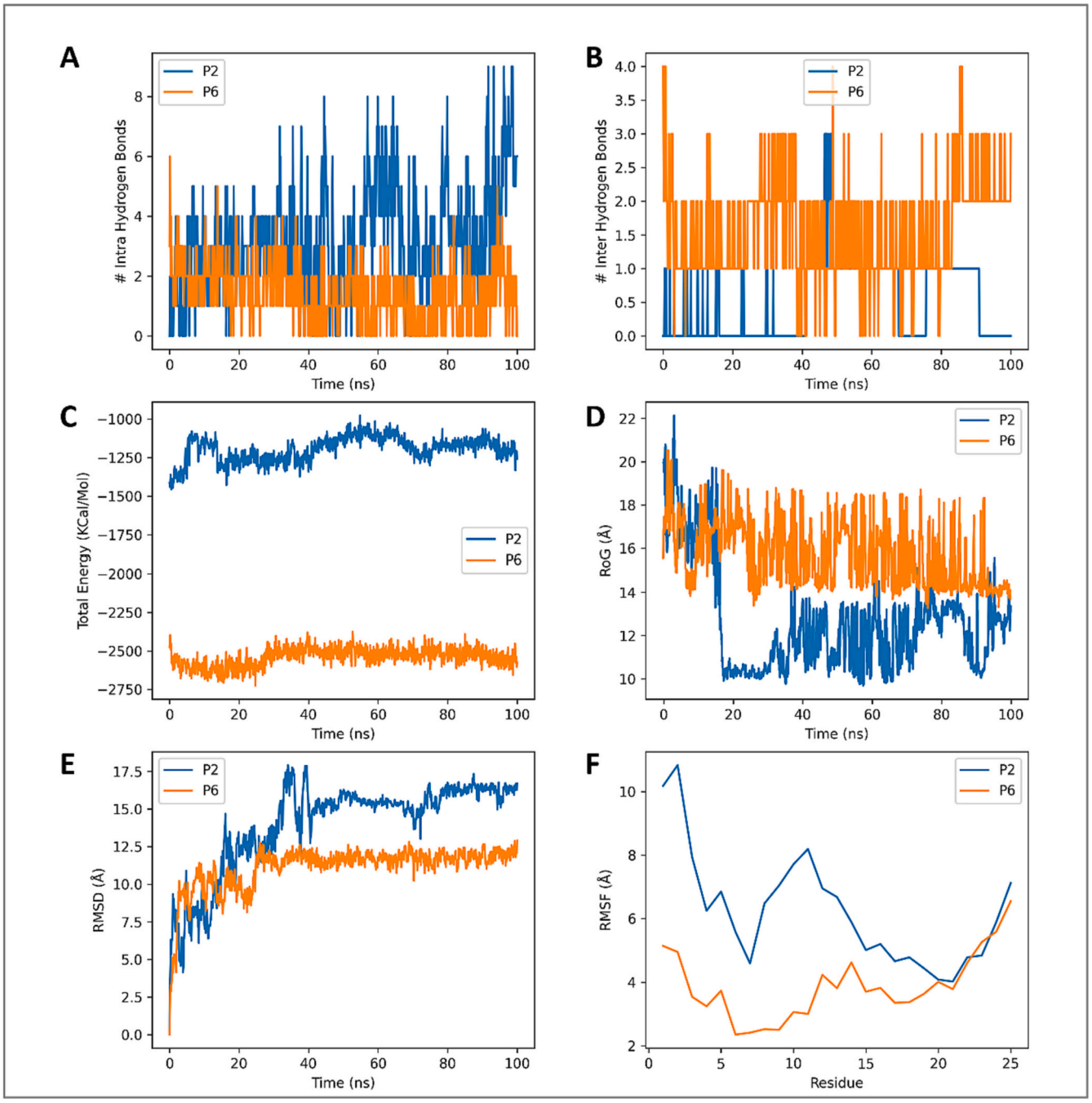

Fig. 2. Molecular Dynamics results for P2 and P6 in an aqueous environment enriched with Ca^{2+}, PO_4^{3-}, and OH^- ions over 100 ns. A Number of intramolecular hydrogen bonds for the peptides. B Number of intermolecular hydrogen bonds for the peptides. C Energy levels over time. D Radius of Gyration for the peptides. E Root-Mean-Square Deviation for the peptides. F Root-Mean-Square Fluctuation for the peptide residues.

between the groups. However, the signal was noisy due to the interference from the filter paper.

S/TEM was used for higher resolution imaging of the samples since the mineralisation oriented at a nanoscale (Fig. 7). It was observed that the peptide groups yielded two-dimensional platelet structures through EDS confirmed to be calcium phosphate (Fig. 7). These flakes were also observable from the high-resolution SEM (Fig. 5). The structures were in the dimensions of a few hundred nanometres and did in some cases, layer itself into lamellar structures. These platelets were not observed for the control group, which seems to only form smaller crystallites that agglomerated (Fig. 7).

In aggregates of minerals, the platelets twisted into needle-like structures (Fig. 8) before they got compacted into clusters. The control group formed wider, thicker crystallites with limited directionality.

4. Discussion

Peptides are becoming frequently employed as tools in tuning the biomedical response in bone regeneration [30]. They are readily synthesised and can be highly potent inducing mineralisation by mimicking the central motif of naturally occurring proteins [31,32]. Benesch, Mano and Reis [33] have identified amelogenins, bone acidic glycoprotein 75, fibronectin and phosphoproteins as essential proteins in acellular mineralisation, and many peptides mimic the motifs of these proteins. Boda

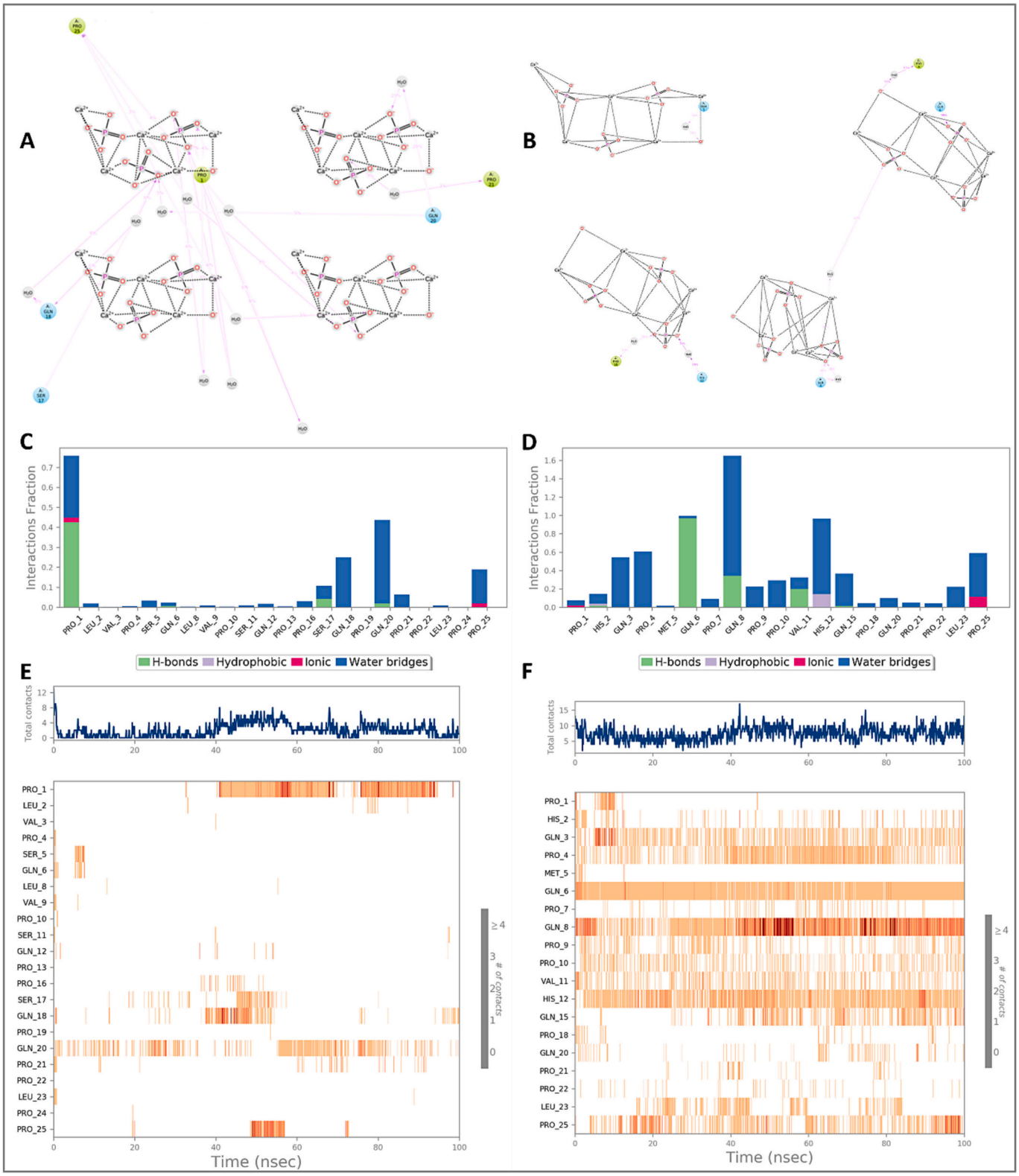

Fig. 3. Molecular Dynamics results for P2 and P6 residual interaction with Ca^{2+}, PO_4^{3-}, and OH^- ions in an aqueous environment over 100 ns. A&B Illustration of interaction for P2 and P6, respectively. C&D Interaction fractions for P2 and P6, respectively. E&F Heat map of the number of molecular interactions for each residual over time for P2 and P6, respectively.

and colleagues [34] loaded calcium-binding BMP-2 mimicking peptide onto pre-mineralised PLGA-collagen-gelatine nanofibers. However, they could not demonstrate statistical significance compared to the pre-mineralised fibers without the BMP-2-peptide. Yarbrough and colleagues [35] investigated peptides comprising repeated sequences of the tripeptide aspartate-serine-serine (DSS) inspired by dentin phosphoprotein. For 8DSS, meaning 8 repeats of the tripeptide sequence, they demonstrated that the peptide efficiently attached to dentin

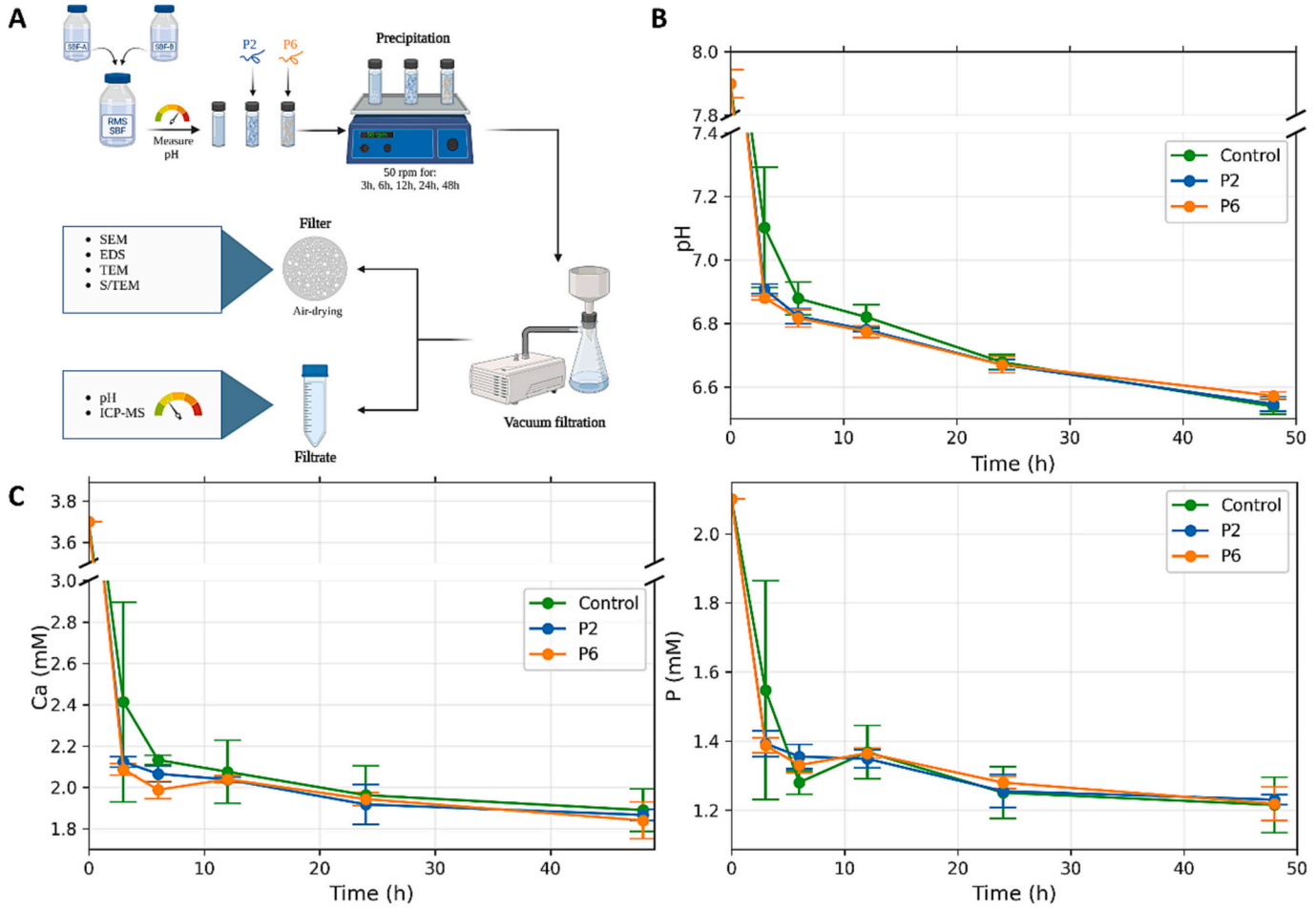

Fig. 4. A Schematic representation of the experimental set-up for the mineralisation study. B pH changes in the RMS SBF with time for the different sample groups. $n = 5$, mean ± SD. C ICP-MS results for calcium (left) and phosphate (right) content in the RMS-SBF solution. $n = 3$, mean ± SD.

surfaces and facilitated the formation of a new mineral layer on top of the dentin, which was facilitated by the peptide adopting its confirmation to expose functional groups on both sides of the interaction plane. Also, Gungormus and colleagues [36] investigated peptides with high binding affinity to hydroxyapatite. Their peptide (HABP1) initially delayed mineralisation but accelerated the conversion from amorphous calcium phosphate to octacalcium phosphate and oriented the mineralisation into platelets-like structures. They believed that the peptide's disordered nature allowed it to bind to hydroxyapatite and regulate new mineralisation efficiently. In two papers by the Goobes group [32,37], they demonstrated that an osteonectin inspired peptide (ON29) could regulate the directionality of the mineral growth into needle-like structures, and they confirmed, by combining computational simulation with solid-state NMR, that the peptide resided between the mineral particles. Similarly to us, Mukherjee and colleagues [38] developed a synthetic peptide, P26, inspired by amelogenin. After agglomerating into nanospherical assemblies, they demonstrated that the peptide induced nucleate apatite formation and guided the formation of thin, lamella-like structures, conforming with the mechanics observed in our work. A key difference from our peptides is that their peptide is not proline-rich. Nevertheless, the morphology of the crystallites was comparable to our results, with a commonality being that theirs and our peptides are disordered in nature.

It has long been theorised that IDPs are vital in mineralisation [39–41]. To fully illuminate the ability of two IDPs (P2 and P6) to nucleate calcium phosphate clusters, the interaction was first observed using molecular dynamics before being experimentally validated. In molecular dynamics simulation, an increase in RMSD of 1–3 is expected from the molecular structure. Meanwhile, anything more than that would be considered larger conformational changes. Our results show greater RMSD with P2 and P6 stabilising at 15.7 Å and 11.8 Å, respectively (mean RMSD between 40 and 100 ns), conforming with the IDP characteristics. Particularly, P2 folded into a stable position, allowing large calcium phosphate clusters to form. P6 remained stretched out due to higher stability in the backbone, favouring more interaction but not necessarily stable mineralisation. This agrees with our pH change observations, where the pH drop is greater for P6 in the first 3 h than for P2. Meanwhile, they are similar after 6 h. After 24 h, there is no significant pH difference between the control and the peptide groups, which can suggest that the peptides either accelerate the mineralisation or are related to the closed system limiting the amount of calcium phosphate that can precipitate. EDS confirmed the crystallites to be calcium phosphate. Moreover, the ICP-MS demonstrate depletion of Ca and P from the solution, meeting the prerequisite for intrinsic osteoinduction [5]. Intrinsic osteoinduction is of significant clinical relevance as it can improve the regeneration of large bone defects or for bone formation in ectopic locations such as during spinal fusion, whereas osteoconduction alone provides too slow regeneration.

Our results also demonstrated that the peptides accelerated mineralisation and regulated the crystal growth, agreeing with former literature on IDPs. Elsharkawy and colleagues [42] demonstrated that elastin-like recombinases (ELRs) could promote mineralisation with unprecedented control and hierarchy. The disordered nature of ELRs triggers the formation of an organised organic framework that can template the growth of hydroxyapatite crystals. Tarasevich and colleagues [28] found that recombinant amelogenin promoted more nucleation of calcium

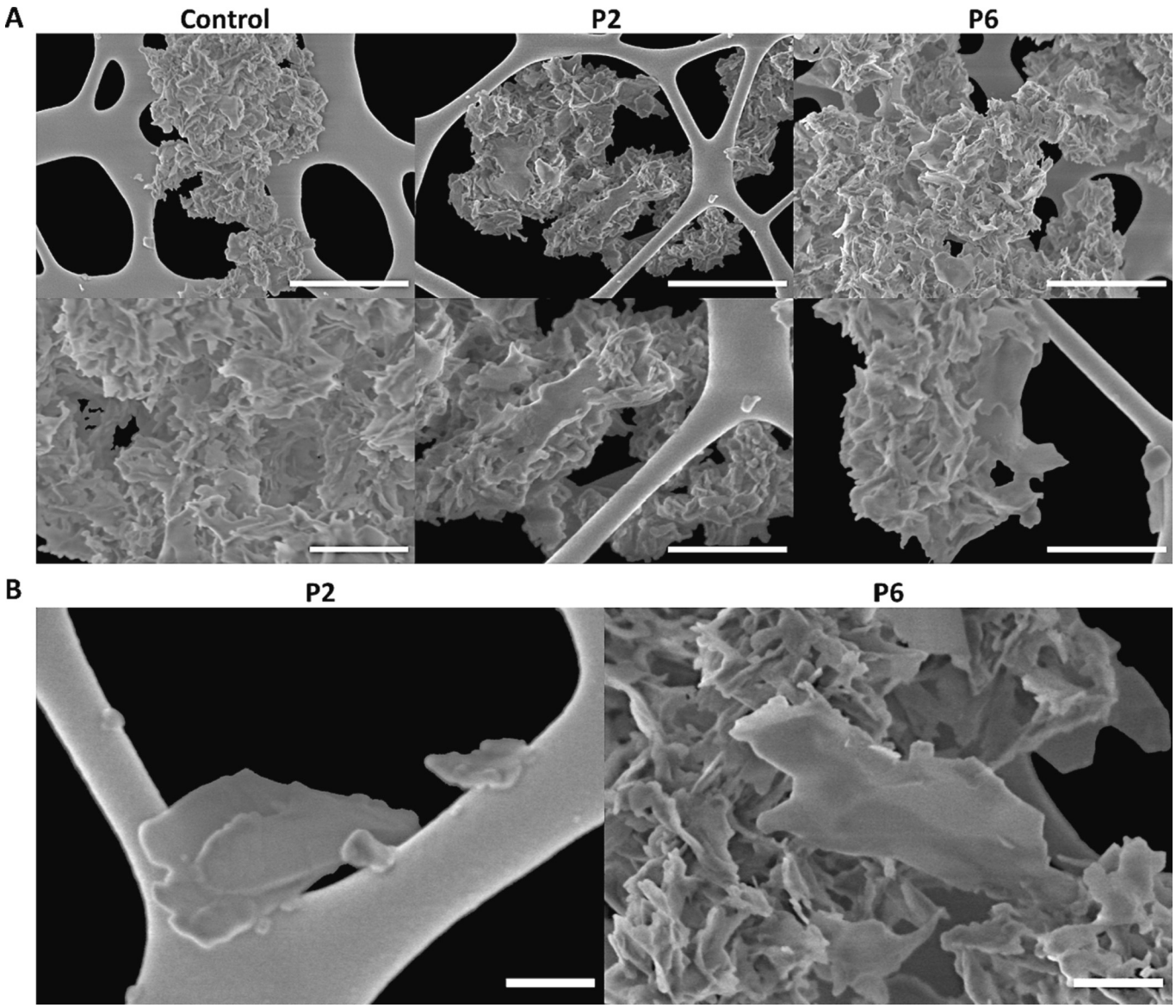

Fig. 5. A SEM images of control, P2, and P6 (left to right) at a magnitude of ×40k (top panel) and ×80K bottom panel after 12 h. Scale bars: Top = 1 μm, bottom = 500 nm. B SEM images of flake-like crystallites forming in the peptide groups were observed. Scale bar: 200 nm.

phosphate compared to control without the proteins through reduced induction time for nucleation. They suggested the mechanism associating amelogenins with nanotemplates, exposing charged functionality on the surface. This agrees with what we observed for P2, which has a high number of intra-hydrogen bonds and folds into a stable position before it nucleates the calcium phosphate cluster through a water bridge with the polar glutamine (residue 20). It is also established that amelogenins provide a directional bias in the crystal growth [43], which can be a similar phenomenon we observed in the peptide groups using S/TEM, where both peptides yielded platelets of minerals.

Previous in vivo studies suggest that P2 can particularly accelerate bone formation [26], agreeing with our observations in our molecular dynamics, where P2 nucleates a larger cluster of calcium phosphate ions. In the animal-model studies, significantly greater formation of mineralised bone was observed only for the P2 enriched bone graft; meanwhile, in this present study, our experimental results suggest greater mineralisation for P6 initially. First, after 48 h, higher mineralisation for P2 is observed than for P6. An explanation can be related to the fact that we used a concentrated SBF solution including only calcium phosphate-related ions. In a biological system, P6 would interact with a series of other macromolecules, which can alter the mineralisation rate. Moreover, RMS-SBF is deprived of precipitation inhibitors such as Mg^{2+} or CO_3^{2-}, and it is 1.5 times more concentrated than the SBF standard composition [44]. This provides a minor bias in this work and can explain why there is a significant mineralisation for both P6 and the control group, not only for P2.

In molecular dynamics simulations, multiple variables can affect the outcome. We chose the force field OPLS-2005 with the water model TIP3P as it is an established and realistic model. However, it is argued that this combination can overestimate the folding stability of IDPs, which is why Yang et al. [45] developed the OPLSIDPTFF force field by introducing a 2D grid-based energy correction map (CMAP) to the OPLS-AA/L force field. Combining this new force field with the water model TIP4P-D demonstrated a clearly improved ability to replicate experimental observation. However, the effect was limited without the change in the water model. Also, Yu and colleagues [46] obtained refined modelling of IDPs with the TIP4P-D water model instead of the TIP3P model. However, in the investigation by Rahmati [26], she compared the P2 and P6 peptides being simulated under either OPLS-AA/L-TIP3P conditions or under OPLSIDPTFF-TIP4P-D + PBS conditions. Using the

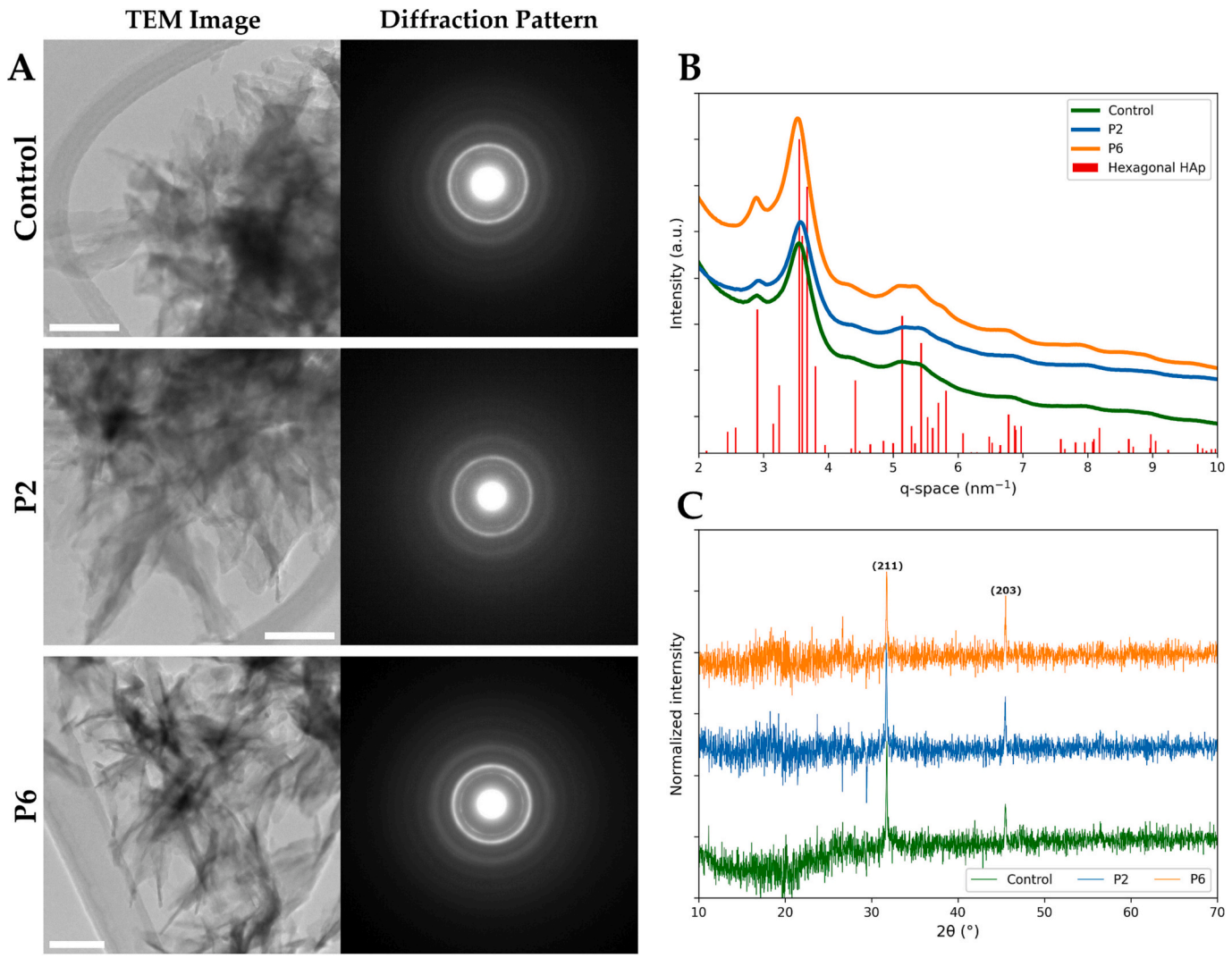

Fig. 6. A TEM image and diffraction pattern for the control group, P2 group, and P6 group after 6 h. Scale bar: 100 nm. B TEM diffraction intensity patterns (average intensity over 360°) against the x-ray pattern expected for a hexagonal calcium hydroxyapatite (HAp – $Ca_5[PO_4]_3[OH]$). C XRD data where the signal from the cellulose filter has been subtracted for the different mineralisation groups. The normalisation was done by subtracting the diffraction pattern of the mixed cellulose esters membrane filter paper where the mineralisation was collected. The data do display clear peaks in the hkl indices 211 and 203.

new force field and TIP4P, the simulation window had to be extended ten-fold, significantly increasing the computational cost, and the Ramachandran plot with MolProbity shows multiple outliers for P6, suggesting unstable simulation results. Moreover, we still observe consensus between our molecular dynamics simulation and experimental validation while using the conventional force field and water model.

5. Conclusion

We have used molecular dynamics and experimental methods to understand how two proline-rich IDPs (P2 and P6) induced mineralisation. The new biomineralisation model presented by Maazouz and colleagues agrees with our in silico molecular dynamics. Our findings also align with Rahmati and colleagues' animal study, demonstrating that in silico modelling combined with SBF studies is a powerful tool for biomaterial research. This suggests that other candidates, such as peptides or ions intended to enhance biomineralisation, can be efficiently studied on the lab bench before expensive animal model studies, also in line with the 3R principle [47]. In our experiments, the peptides adapted to the ion-rich surroundings to facilitate the nucleation of calcium phosphate crystals, which translates to accelerated mineralisation. Mainly, P2 seemed to fold into a stable structure that provided a template for anchoring a large cluster of calcium phosphate. In the experimental model, we observed that the peptide groups depleted the local surroundings for calcium and phosphorous ions significantly quicker than the control group, suggesting accelerated mineralisation. Moreover, this is a prerequisite for intrinsic osteoinduction. When evaluating the mineralisation, it was observed that the peptides provided thin platelet mineralisation that, in clusters twisted itself into needle-like structures or stacked into lamellar structures, indicating that the peptides regulate the growth of minerals. Meanwhile, the control group yielded thicker mineral clusters. The flakes are also favourable for remodelling into native human bone. Based on the results presented in this work, we have concluded that the peptides accelerate and regulate mineralisation and can induce intrinsic osteoinduction if integrated into therapies for bone regeneration.

CRediT authorship contribution statement

Øystein Øvrebø: Writing – original draft, Methodology, Investigation, Formal analysis, Data curation. **Angela De Lauretis:** Writing – original draft, Investigation, Formal analysis, Data curation. **Qianli Ma:** Writing – review & editing, Methodology, Formal analysis. **Ståle Petter**

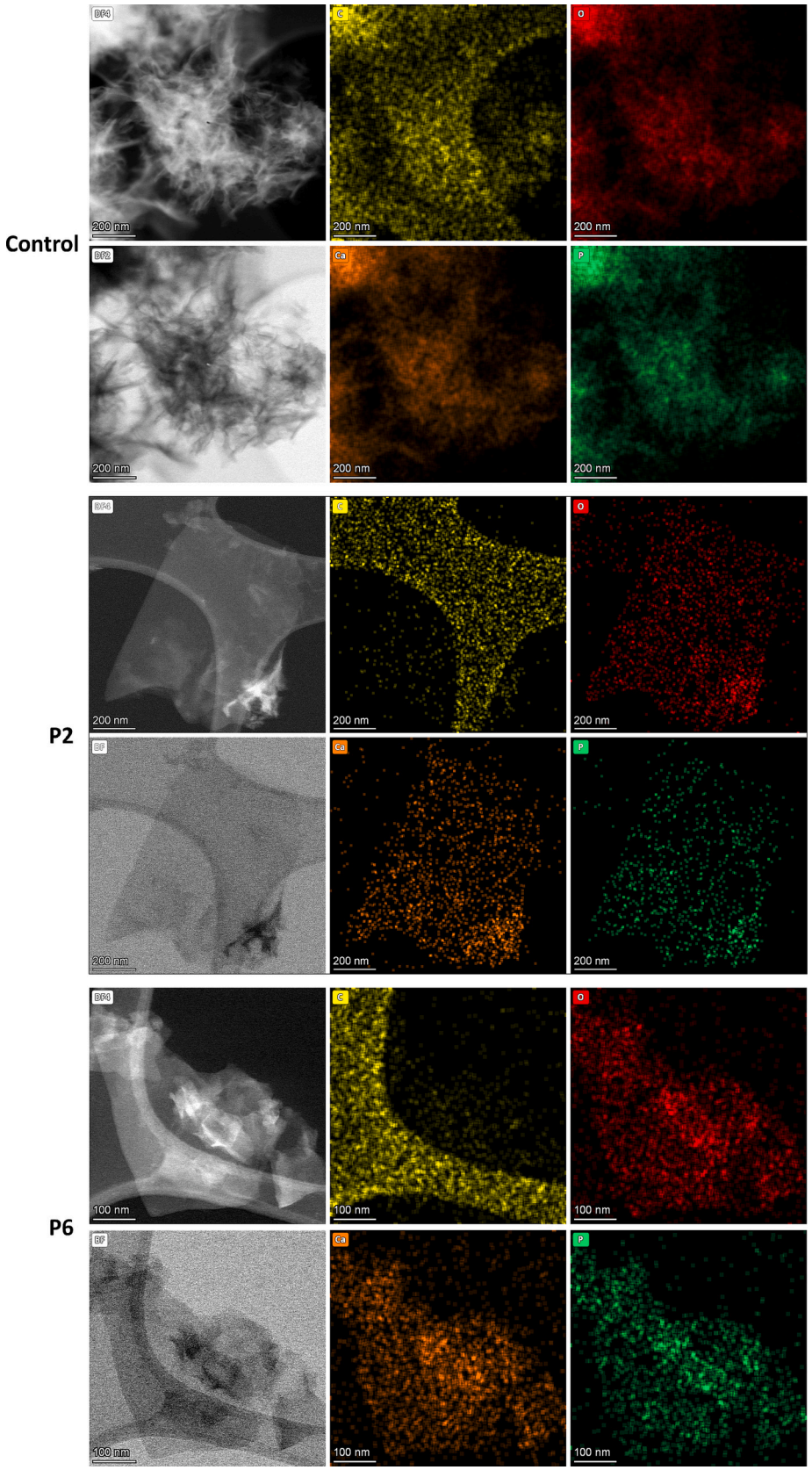

Fig. 7. S/TEM (BF: Bright field; DF: Dark field) and EDS of platelet-like calcium phosphate crystallites from the P2 group (middle) and the P6 group (bottom), which was not observed for the control (top). Ca, P, and O are from the calcium phosphate, and C is from the carbon tape of the bottom of the copper grid.

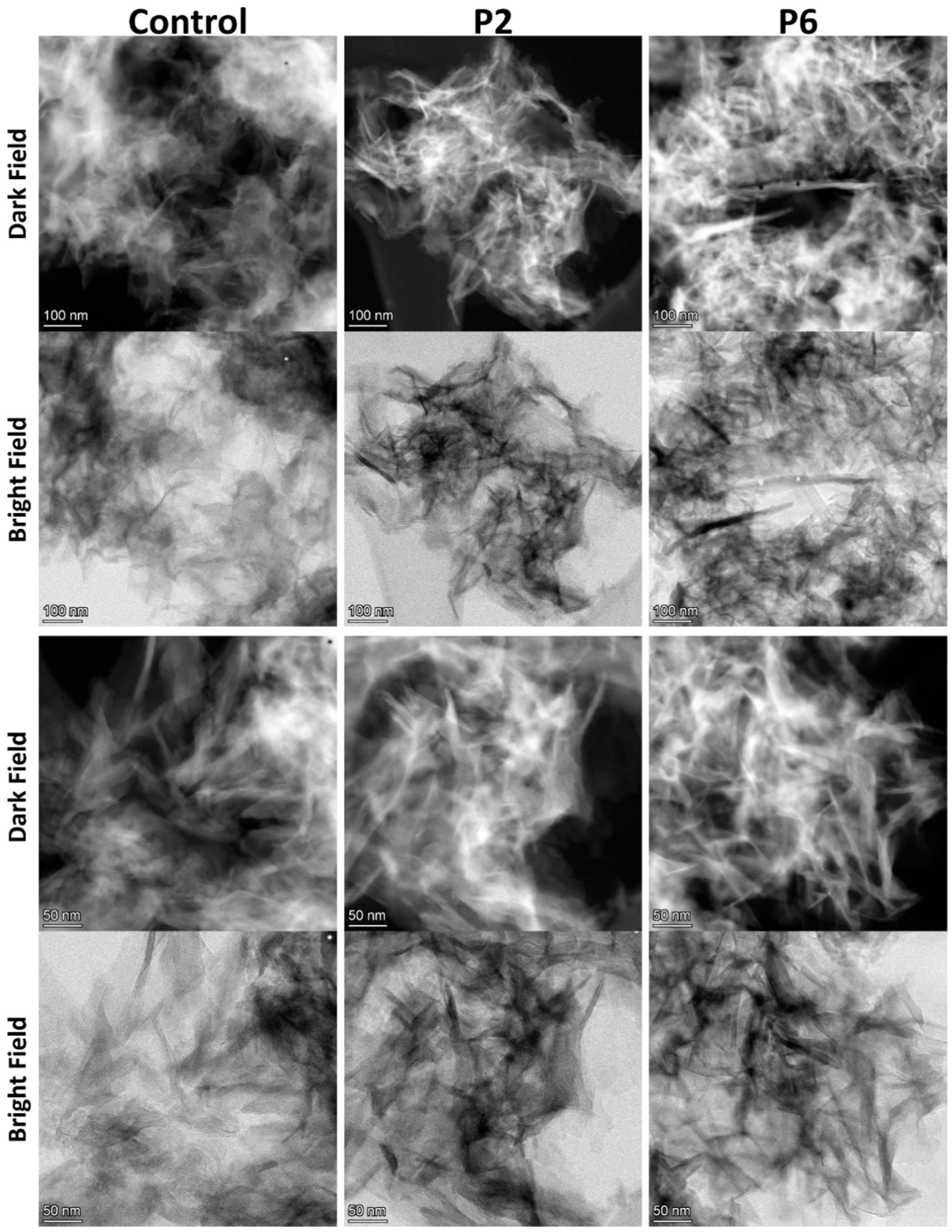

Fig. 8. S/TEM bright and dark field of mineralisation from control samples (RMS-SBF only) and the peptide solutions (P2 & P6).

Lyngstadaas: Writing – review & editing, Methodology, Formal analysis. **Giuseppe Perale:** Writing – review & editing, Methodology, Formal analysis. **Ola Nilsen:** Writing – review & editing, Methodology, Investigation. **Filippo Rossi:** Writing – original draft, Supervision, Methodology, Formal analysis. **Håvard J. Haugen:** Writing – original draft, Supervision, Methodology, Investigation, Formal analysis, Conceptualization.

Declaration of competing interest

The authors declare the following financial interests/personal relationships which may be considered as potential competing interests: The authors declare no financial and personal relationships with other people or organisations that could inappropriately influence bias to this work. IPR rights of the consensus peptides (US Patent US8367602B2 and connected titles) belong to Industrie Biomediche Insubri SA (Switzerland), where Giuseppe Perale is a founding shareholder and the executive vice president. The patent related to the consensus peptides was invented by Ståle Petter Lyngstadaas but has since been sold to Industrie Biomediche Insubri SA. NuPep AS, owned solely by Øystein Øvrebø, has a licencing right to the consensus peptides IPR above.

Data availability

Data will be made available on request.

Acknowledgements

The authors appreciate research funding from the European Commission through Eureka E!914. ØØ and HJH acknowledge additional funding from the Norwegian Research Council grant nr. 327512, 331752 and 332148. HJH and QM acknowledge funding from the EEA grant number LV-RESEARCH-0005 "Eggshell". We thank Walace Peterle Soares Kierulf-Vieira and Siri Simonsen for assistance with SEM, and Anuj Pokle for assistance with TEM and S/TEM.

Appendix A. Supplementary data

Supplementary data to this article can be found online at https://doi.org/10.1016/j.bioadv.2024.213801.

References

[1] E. Garcia-Gareta, M.J. Coathup, G.W. Blunn, Osteoinduction of bone grafting materials for bone repair and regeneration, Bone 81 (2015) 112–121.
[2] Ø. Øvrebø, G. Perale, J.P. Wojciechowski, C. Echalier, J.R. Jeffers, M.M. Stevens, H. J. Haugen, F. Rossi, Design and clinical application of injectable hydrogels for musculoskeletal therapy, Bioeng. Transl. Med. 7 (2) (2022) e10295.
[3] T. Albrektsson, C. Johansson, Osteoinduction, osteoconduction and osseointegration, Eur. Spine J. 10 (2) (2001) S96–S101.
[4] R. Miron, Y. Zhang, Osteoinduction: a review of old concepts with new standards, J. Dent. Res. 91 (8) (2012) 736–744.
[5] M. Bohner, R.J. Miron, A proposed mechanism for material-induced heterotopic ossification, Mater. Today 22 (2019) 132–141.
[6] N. Reznikov, M. Bilton, L. Lari, M.M. Stevens, R. Kroger, Fractal-like hierarchical organisation of bone begins at the nanoscale, Science 360 (6388) (2018) eaao2189.
[7] M.M. Stevens, Biomaterials for bone tissue engineering, Mater. Today 11 (5) (2008) 18–25.
[8] M.E. Launey, M.J. Buehler, R.O. Ritchie, On the mechanistic origins of toughness in bone, Annu. Rev. Mater. Res. 40 (2010) 25–53.
[9] A. Ural, D. Vashishth, Hierarchical perspective of bone toughness–from molecules to fracture, Int. Mater. Rev. 59 (5) (2014) 245–263.
[10] S. Pang, H.P. Schwarcz, I. Jasiuk, Interfacial bonding between mineral platelets in bone and its effect on mechanical properties of bone, J. Mech. Behav. Biomed. Mater. 113 (2021) 104132.
[11] L. Kalmar, D. Homola, G. Varga, P. Tompa, Structural disorder in proteins brings order to crystal growth in biomineralization, Bone 51 (3) (2012) 528–534.
[12] S. Elsharkawy, A. Mata, Hierarchical biomineralization: from nature's designs to synthetic materials for regenerative medicine and dentistry, Adv. Healthc. Mater. 7 (18) (2018) 1800178.
[13] K. Delak, C. Harcup, R. Lakshminarayanan, Z. Sun, Y. Fan, J. Moradian-Oldak, J. S. Evans, The tooth enamel protein, porcine amelogenin, is an intrinsically disordered protein with an extended molecular configuration in the monomeric form, Biochemistry 48 (10) (2009) 2272–2281.
[14] P.-A. Fang, J.F. Conway, H.C. Margolis, J.P. Simmer, E. Beniash, Hierarchical self-assembly of amelogenin and the regulation of biomineralization at the nanoscale, Proc. Natl. Acad. Sci. 108 (34) (2011) 14097–14102.
[15] T. Wald, F. Spoutil, A. Osickova, M. Prochazkova, O. Benada, P. Kasparek, L. Bumba, O.D. Klein, R. Sedlacek, P. Sebo, Intrinsically disordered proteins drive enamel formation via an evolutionarily conserved self-assembly motif, Proc. Natl. Acad. Sci. 114 (9) (2017) E1641–E1650.
[16] S.P. Lyngstadaas, J.C. Wohlfahrt, S.J. Brookes, M.L. Paine, M.L. Snead, J. E. Reseland, Enamel matrix proteins; old molecules for new applications, Orthod. Craniofacial Res. 12 (3) (2009) 243–253.
[17] M. Rubert, J.M. Ramis, J. Vondrasek, A. Gaya, S.P. Lyngstadaas, M. Monjo, Synthetic peptides analogue to enamel proteins promote osteogenic differentiation of MC3T3-E1 and mesenchymal stem cells, J. Biomater. Tissue Eng. 1 (2) (2011) 198–209.
[18] J.M. Ramis, M. Rubert, J. Vondrasek, A. Gaya, S.P. Lyngstadaas, M. Monjo, Effect of enamel matrix derivative and of proline-rich synthetic peptides on the differentiation of human mesenchymal stem cells toward the osteogenic lineage, Tissue Eng. A 18 (11–12) (2012) 1253–1263.
[19] M. Rubert, M. Monjo, S.P. Lyngstadaas, J.M. Ramis, Effect of alginate hydrogel containing polyproline-rich peptides on osteoblast differentiation, Biomed. Mater. 7 (5) (2012).
[20] M. Rubert, H. Pullisaar, M. Gómez-Florit, J.M. Ramis, H. Tiainen, H.J. Haugen, S. P. Lyngstadaas, M. Monjo, Effect of TiO2 scaffolds coated with alginate hydrogel containing a proline-rich peptide on osteoblast growth and differentiation in vitro, J. Biomed. Mater. Res. A 101A (6) (2013) 1768–1777.
[21] H.J. Haugen, P. Basu, M. Sukul, J.F. Mano, J.E. Reseland, Injectable biomaterials for dental tissue regeneration, Int. J. Mol. Sci. 21 (10) (2020) 3442–3475.
[22] S.P. Lyngstadaas, J.E. Ellingsen, in: U. States (Ed.), Consensus Peptides and a Method for Inducing Biomineralization, Industrie Biomediche Insubri SA, 2013.
[23] G. Perale, M. Monjo, J.M. Ramis, Ø. Øvrebø, F. Betge, P. Lyngstadaas, H.J. Haugen, Biomimetic biomolecules in next generation xeno-hybrid bone graft material show enhanced in vitro bone cells response, J. Clin. Med. 8 (12) (2019) 2159–2177.
[24] H. Zhu, M. Gomez, J. Xiao, G. Perale, F. Betge, S.P. Lyngstadaas, H.J. Haugen, Xenohybrid bone graft containing intrinsically disordered proteins shows enhanced in vitro bone formation, ACS Appl. Bio Mater. 3 (4) (2020) 2263–2274.
[25] H. Zhu, V.H. Blahnova, G. Perale, J. Xiao, F. Betge, F. Boniolo, E. Filova, S. P. Lyngstadaas, H.J. Haugen, Xeno-hybrid bone graft releasing biomimetic proteins promotes osteogenic differentiation of hMSCs, Front. Cell Dev. Biol. 8 (2020) 619111.
[26] M. Rahmati, S. Stötzel, T. El Khassawna, C. Mao, A. Ali, J.C. Vaughan, K. Iskhahova, D.C. Florian Wieland, A.G. Cantalapiedra, G. Perale, F. Betge, E. P. Dillon, S.P. Lyngstadaas, H.J. Haugen, Intrinsically disordered peptides enhance regenerative capacities of bone composite xenografts, Mater. Today 63 (2021) 63–79.
[27] Y. Maazouz, G. Chizzola, N. Döbelin, M. Bohner, Cell-free, quantitative mineralization measurements as a proxy to identify osteoinductive bone graft substitutes, Biomaterials (2021) 120912.
[28] B.J. Tarasevich, C.J. Howard, J.L. Larson, M.L. Snead, J.P. Simmer, M. Paine, W. J. Shaw, The nucleation and growth of calcium phosphate by amelogenin, J. Cryst. Growth 304 (2) (2007) 407–415.
[29] M. Markovic, B.O. Fowler, M.S. Tung, Preparation and comprehensive characterization of a calcium hydroxyapatite reference material, J. Res. Natl. Inst. Stand. Technol. 109 (6) (2004) 553.
[30] H.J. Haugen, S.P. Lyngstadaas, F. Rossi, G. Perale, Bone grafts: which is the ideal biomaterial? J. Clin. Periodontol. 46 (2019) 92–102.
[31] M. Bermúdez, L. Hoz, G. Montoya, M. Nidome, A. Pérez-Soria, E. Romo, U. Soto-Barreras, J. Garnica-Palazuelos, M. Aguilar-Medina, R. Ramos-Payán, Bioactive synthetic peptides for oral tissues regeneration, Front. Mater. 8 (2021) 655495.
[32] T. Iline-Vul, I. Matlahov, J. Grinblat, K. Keinan-Adamsky, G. Goobes, Changes to the disordered phase and apatite crystallite morphology during mineralization by an acidic mineral binding peptide from osteonectin, Biomacromolecules 16 (9) (2015) 2656–2663.
[33] J. Benesch, J.F. Mano, R.L. Reis, Proteins and their peptide motifs in acellular apatite mineralization of scaffolds for tissue engineering, Tissue Eng. B Rev. 14 (4) (2008) 433–445.
[34] S.K. Boda, Y. Almoshari, H. Wang, X. Wang, R.A. Reinhardt, B. Duan, D. Wang, J. Xie, Mineralized nanofiber segments coupled with calcium-binding BMP-2 peptides for alveolar bone regeneration, Acta Biomater. 85 (2019) 282–293.
[35] D.K. Yarbrough, E. Hagerman, R. Eckert, J. He, H. Choi, N. Cao, K. Le, J. Hedger, F. Qi, M. Anderson, Specific binding and mineralization of calcified surfaces by small peptides, Calcif. Tissue Int. 86 (2010) 58–66.
[36] M. Gungormus, H. Fong, I.W. Kim, J.S. Evans, C. Tamerler, M. Sarikaya, Regulation of in vitro calcium phosphate mineralization by combinatorially selected hydroxyapatite-binding peptides, Biomacromolecules 9 (3) (2008) 966–973.
[37] I. Matlahov, T. Iline-Vul, M. Abayev, E.M. Lee, M. Nadav-Tsubery, K. Keinan-Adamsky, J.J. Gray, G. Goobes, Interfacial mineral–peptide properties of a mineral binding peptide from osteonectin and bone-like apatite, Chem. Mater. 27 (16) (2015) 5562–5569.
[38] K. Mukherjee, Q. Ruan, S. Nutt, J. Tao, J.J. De Yoreo, J. Moradian-Oldak, Peptide-based bioinspired approach to regrowing multilayered aprismatic enamel, ACS Omega 3 (3) (2018) 2546–2557.
[39] A.L. Boskey, E. Villarreal-Ramirez, Intrinsically disordered proteins and biomineralization, Matrix Biol. 52 (2016) 43–59.
[40] P. Tompa, Intrinsically unstructured proteins, Trends Biochem. Sci. 27 (10) (2002) 527–533.
[41] J. Moradian-Oldak, A. George, Biomineralization of enamel and dentin mediated by matrix proteins, J. Dent. Res. 100 (10) (2021) 1020–1029.
[42] S. Elsharkawy, M. Al-Jawad, M.F. Pantano, E. Tejeda-Montes, K. Mehta, H. Jamal, S. Agarwal, K. Shuturminska, A. Rice, N.V. Tarakina, Protein disorder–order interplay to guide the growth of hierarchical mineralized structures, Nat. Commun. 9 (1) (2018) 2145–2156.
[43] B.L. Foster, T.E. Popowics, H.K. Fong, M.J. Somerman, Advances in defining regulators of cementum development and periodontal regeneration, Curr. Top. Dev. Biol. 78 (2007) 47–126.
[44] Y. Maazouz, I. Rentsch, B. Lu, B.L.G. Santoni, N. Doebelin, M. Bohner, In vitro measurement of the chemical changes occurring within β-tricalcium phosphate bone graft substitutes, Acta Biomater. 102 (2020) 440–457.
[45] S. Yang, H. Liu, Y. Zhang, H. Lu, H. Chen, Residue-specific force field improving the sample of intrinsically disordered proteins and folded proteins, J. Chem. Inf. Model. 59 (11) (2019) 4793–4805.
[46] L. Yu, D.-W. Li, R. Brüschweiler, Balanced amino-acid-specific molecular dynamics force field for the realistic simulation of both folded and disordered proteins, J. Chem. Theory Comput. 16 (2) (2019) 1311–1318.
[47] A. Vitale, L. Ricceri, The principle of the 3Rs between aspiration and reality, Front. Physiol. 13 (2022) 914939.